Applications of Polynomial Chaos-Based Cokriging to Aerodynamic Design Optimization Benchmark Problems

Jethro Nagawkar* and Leifur Leifsson[†] *Iowa State University, Ames, Iowa, 50011, USA*

Xiaosong Du [‡]
University of Michigan, Ann Arbor, Michigan, 48109, USA

In this work, the polynomial chaos-based Cokriging (PC-Cokriging) is applied to a benchmark aerodynamic design optimization problem. The aim is to perform fast design optimization using this multifidelity metamodel. Multifidelity metamodels use information at multiple levels of fidelity to make accurate and fast predictions. Higher amount of lower fidelity data can provide important information on the trends to a limited amount of high-fidelity (HF) data. The PC-Cokriging metamodel is a multivariate version of the polynomial chaos-based Kriging (PC-Kriging) metamodel and its construction is similar to Cokriging. It combines the advantages of the interpolation-based Kriging metamodel and the regression-based polynomial chaos expansions (PCE). In the work the PC-Cokriging model is compared to other metamodels namely PCE, Kriging, PC-Kriging and Cokriging. These metamodel are first compared in terms of global accuracy, measured by root mean squared error (RMSE) and normalized RMSE (NRMSE) for different sample sets, each with an increasing number of HF samples. These metamodels are then used to find the optimum. Once the optimum design is found computational fluid dynamics (CFD) simulations are rerun and the results are compared to each other. In this study a drag reduction of 73.1 counts was achieved. The multifidelity metamodels required 19 HF samples along with 1,055 low-fidelity to converge to the optimum drag value of 129 counts, while the single fidelity models required 155 HF samples to do the same.

Nomenclature

airfoil cross-sectional area, [-] baseline airfoil cross-sectional area, [-] $A_{baseline}$ speed of sound in air, [m/s] chord length, [-] cdrag coefficient, $\frac{d}{q_{\infty}c}$, [-] skin friction coefficient, $\frac{\tau_w}{q_{\infty}}$, [-] C_d C_f lift coefficient, $\frac{1}{q_{\infty}c}$, [-] pitching moment coefficient, $\frac{m}{q_{\infty}c^2}$, [-] C_l C_m pressure coefficient, $\frac{p-p_{\infty}}{q_{\infty}}$, [-] drag count, 1E-4 ΔC_d lift count, 1E-2 ΔC_l = drag force, [N] lift force, [N] lower bounds of the design variables pitching moment, [N/m] m freestream Mach number, $\frac{V_{\infty}}{a}$, [-] M_{∞} static pressure on airfoil surface, [N/m²]

^{*}Ph.D. Student, Department of Aerospace Engineering, AIAA Student Member.

[†]Assistant Professor, Department of Aerospace Engineering, AIAA Senior Member.

[‡]Post-Doctoral Research Fellow, Department of Aerospace Engineering, AIAA Student Member.

 p_{∞} = freestream static pressure, [N/m²]

 q_{∞} = freestream dynamic pressure, $0.5\rho_{\infty}V_{\infty}^2$, [N/m²]

Re = Reynolds number, $\frac{\rho_{\infty}V_{\infty}c}{\mu_{\infty}}$, [-]

u = upper bounds of the design variables

 V_{∞} = freestream air velocity, [m/s] **x** = vector of design variables

 \mathbf{x}_c = vector of x/c location design variables

 $\bar{\mathbf{x}}^{(0)}$ = baseline design variable vector

X = sampling plan vector

y = observations of the sampling plan y_{testing} = observations at testing point

 $\hat{\mathbf{y}}_{testing}$ = metamodel responses at testing points

 y^+ = non-dimensionalized first layer cell thickness, [-]

 α = angle of attack, [degrees]

 μ_{∞} = freestream viscosity of air, [Ns/m²] ρ_{∞} = freestream air density, [kg/m³] τ_{w} = wall shear stress, [N/m²]

I. Introduction

Aerodynamic design optimization (ADO) is an important part of designing complex physical systems such as aeroplanes, cars, trains and wind turbines. The use of computer simulations in the design process is increasingly becoming the norm. This involves solving costly, but accurate HF partial differential equations (PDEs). HF simulations are important as it is essential to capture the complex nonlinearities within the system in order to represent its performance accurately. Low-fidelity (LF) PDEs may not be able to capture these nonlinearities accurately, leading to poor design choices.

Traditional methods in ADO have relied heavily on expensive HF simulations in order to calculate the cost function and constraint values [1–5] accurately. The most popular of these methods has been the use of a gradient based search algorithm, where the gradients are calculated using adjoints [4–8]. Another way of solving ADO problems is using metamodeling (also know as surrogate modeling) [9–16]. It consists of two types: data-fit methods [17, 18] and multifidelity methods [19]. Data-fit methods involve fitting a response surface through the evaluated cost function value at sampled points in the design space. This method typically requires large number of sample points, but is versatile and can handle highly nonlinear data. Methods include Kriging [20–23], polynomial chaos expansions (PCE) [24], and support vector regression [25]. Multifidelity metamodeling [19] alleviates the computational burden by using information from multiple fidelities. A large number of LF data can be used to provide useful information on the trends to a small number of HF data. LF models are typically approximations of the HF models. They can be simplified governing equations [26], projection-based methods [27], and data-fit methods [20].

Numerous works on metamodeling-based ADO can be found in literature for both deterministic and robust design. Jonsson et al. [9] used space mapping to optimize the shape of trawl-doors. Cokriging was used by Koziel et al. [10] and Amrit et al. [11] to expedite multi-objective ADO. Reinforcement learning and transfer learn was used by Yan et al. [15] to perform ASO on missile surfaces. A reduction in CFD calls by 62.5% was reported by them. Bouhlel et al. [16] used Kriging and Kriging with partial least squares (KPLS) to perform efficient global optimization on analytical functions and a benchmark automotive problem. These studies have been performed for deterministic optimum design. Shah et al. [12] performed multifidelity robust design optimization of a NACA 2412 airfoil under mixed uncertainty. Two uncertainty variables, the Mach number and the geometric parameter of the thickness distribution of the airfoil were used in their study. Deep belief network along with a particle swarm optimizer was used by Tao and Sun [14] to perform robust design optimization on a RAE2822 airfoil as well as a DLR-F6 wing body model for uncertainty in Ma.

In this work, the polynomial chaos-based Cokriging (PC-Cokriging) developed by Du and Leifsson [28] is used to perform fast ADO of airfoils. PC-Cokriging is a multivariate extension of PC-Kriging [29–31]. It is constructed similar to the Cokriging [20] metamodel, with PC-Kriging used in place of Kriging [20]. Benchmark case II developed by the AIAA Aerodynamic Optimization Design Discussion Group (ADODG) is selected for this study. Numerous work on this benchmark case has already been done [4, 32–38].

The paper is organised in the following sequence. The next section describes the method used to construct the PC-Cokiriging metamodel. In the following section, the PC-Cokiriging metamodel is applied to the benchmark case II

for fast design optimization. In this section, it has been benchmarked against other metamodeling methods such as PCE [39], Kriging [20], PC-Kriging [30] and Cokriging [20]. The last section presents the conclusions and suggestions for future work.

II. Methods

This section describes the methods used to construct the PC-Cokriging multifidelity metamodel. The following subsections describe the metamodel algorithm, the sampling plan, metamodeling, validation and ASO for the benchmark case.

A. Multifidelity metamodel algorithm

A flowchart of the PC-Cokriging based multifidelity metamodel algorithm is shown in Fig. 1. The process starts by sampling the design space at a fixed number of design points. The LF model is evaluated at all these samples, while the HF model is only evaluated at a subset of them. The multifidelity metamodel is then constructed by combining the HF and LF observations. Finally, the metamodel is validated with a separate set of testing data. If the metamodel does not meet the testing criteria, it is resampled with a larger number of HF data and the same procedure is redone. Once, the metamodel is sufficiently accurate, the optimum design is found.

B. Sampling plan

The first step involved in constructing the metamodel is sampling. In order to capture the trend of the true cost function, the design space needs to be sampled at certain fixed combinations of the design variables (DVs). The metamodel is then constructed using this sampled data. In this work, the Latin Hypercube sampling (LHS) [40] is used for generating both the training and testing points. The LF model is evaluated at all the training points, while the HF model is evaluated only at a limited subset of the training points. This is because of the high computational cost of HF model. The HF model is also evaluated at all the testing points in order to test the prediction accuracy of the metamodel.

C. Metamodeling

In this work, the PC-Cokriging metamodel proposed by Du and Leifsson [28] is used. This metamodel is a multivariate version of the PC-Kriging [29, 30] model, which is constructed in a similar method as Cokriging [41–43]. A PC-Kriging model combines the PCE [39] and Kriging [21, 23, 44] methods. The regression-based PCE captures the global trend

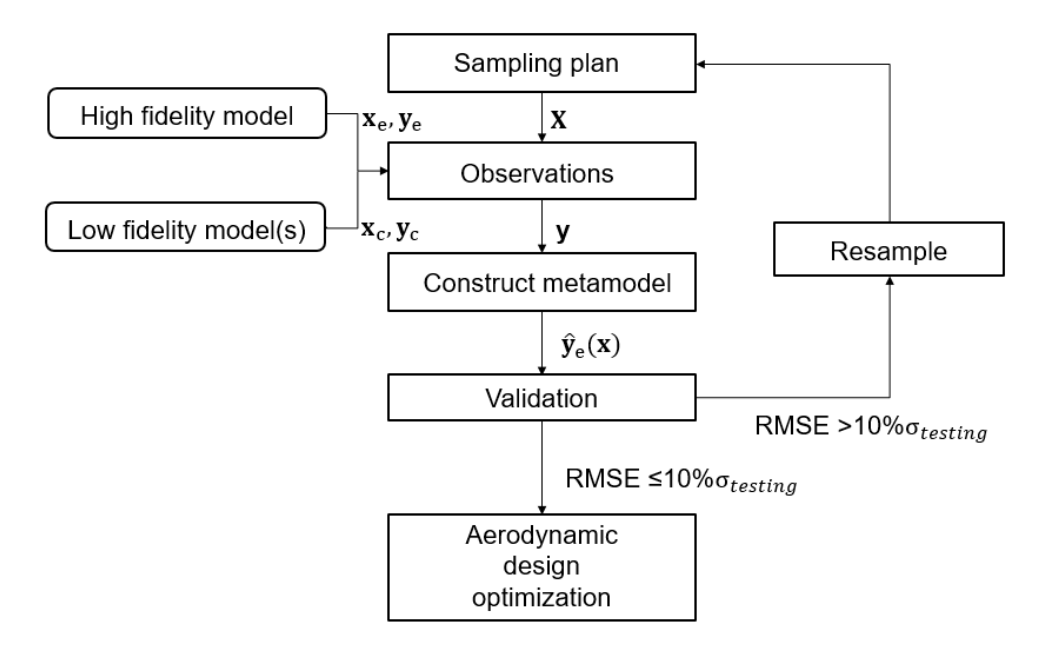


Figure 1 Flowchart of the PC-Cokriging based ADO.

of the model well, while the interpolation-based Kriging captures the local deviations. This makes the PC-Kriging metamodel more effective as it combines the strengths of both the models. To construct a Cokriging model, a Kriging approximation of the LF model multiplied by a scaling factor and another Kriging approximation of the difference of HF and LF model outputs is combined. For PC-Cokriging, the Kriging approximation is replaced by the PC-Kriging approximation. The generaized PC-Cokriging formula is given by

$$M^{PC-CoK}(\mathbf{x}) = \rho M_{LF}^{PCK}(\mathbf{x}) + M_{Diff}^{PCK}(\mathbf{x}), \tag{1}$$

where $M_{\rm LF}^{PCK}$ is the PC-Kriging approximation of the LF data, and $M_{\rm Diff}^{PCK}$ is the PC-Kriging approximation of the difference of the output of the HF and LF data. PC-Kriging is used to construct the $M_{\rm LF}^{PCK}$ and $M_{\rm Diff}^{PCK}$ terms. A detailed description of the construction of these terms can be found in Du and Leifsson [28]. The following steps are used to construct the PC-Cokriging metamodel:

- 1) A least angle regression (LARS) [45] is used to select the most correlated orthogonal bases for PCE on the LF training data;
- 2) The bases selected from Step 1 are plugged into a universal Kriging metamodel to construct the PC-Kriging model on the LF data;
- 3) At the HF training points, another PC-Kriging metamodel is constructed for the difference model, $M_{\text{Diff}}(\mathbf{x}_{\text{HF}})$;
- 4) The unknown parameters are solved for and the predictor is constructed in the same way as the Cokriging metamodel [42].

The hyperparameters present in the Gaussian exponential spatial correlation function [46] and the Matern-5/2 covariance function [47] of the kriging based metamodels needs to be tuned. This is done during the training phase by finding the maximum likelihood estimate on the training data. This hyperparameter is found using the differential evolution algorithm in SciPy [48]. The other hyperparameter, the order of the PCE, which is used in the PCE based metamodels are found iteratively. The metamodels are generated and tested by varying the order from one to six. The order with the lowest testing error is chosen.

D. Validation

To validate the metamodels, the root mean squared error (RMSE) given by

RMSE =
$$\sqrt{\sum_{i=1}^{n_t} (\hat{y}_{testing}^{(i)} - y_{testing}^{(i)})^2 / n_t},$$
 (2)

and the normalized RMSE (NRMSE) given by

$$NRMSE = RMSE/(max(\mathbf{y}_{testing}) - min(\mathbf{y}_{testing})), \tag{3}$$

is used in this work. Here $\hat{y}_{testing}^{(i)}$ and $y_{testing}^{(i)}$ are the metamodel estimation and HF observation of the *i*th testing point, respectively. $\max(\mathbf{y}_{testing})$ and $\min(\mathbf{y}_{testing})$ refers to the maximum and minimum HF values observed amongst all testing points respectively. Note that in this study the training and testing data are generated from two different LHS. n_t is the total number of testing data sets. An RMSE less than or equal to $10\%\sigma_{testing}$ (standard deviation of testing points) is taken as the acceptable global accuracy criterion in this work.

E. Metamodel based optimization

Once the metamodel reaches the required global accuracy, it is then used to find the optima. For this study a multi-start gradient based search algorithm is used to find the minima. The optimizer used is the sequential least squares programming (SLSQP) optimizer available in SciPy [48]. The choice of using different initial starting points is to avoid the optimizer from getting stuck in a local minima. For this study, 40 initial starting point are used. These starting points are generated using LHS. The lowest obtained minima is reported in this study.

III. Benchmark Case II

For this research work, benchmark case II developed by the AIAA Aerodynamic Optimization Design Discussion Group (ADODG) is selected. This section begins with the problem formulation followed by the design variables used to parameterize the airfoil. The CFD setup and validation is then discussed as well as the metamodel generation and validation. Finally, the optimization results are presented.

A. Problem formulation

The objective of this case is to minimize the drag coefficient (C_d) of a RAE 2822 airfoil in viscous flow of freestream Mach number (M_∞) equal to 0.734 subject to a fixed lift coefficient (C_l) of 0.824 as well as pitching moment coefficient (C_m) and area constraints.

The optimization problem is stated as

$$\min_{\mathbf{l} < \mathbf{x} < \mathbf{u}} C_d \tag{4}$$

subject to the equality constraint

$$C_l = 0.824$$
 (5)

and inequality constraints

$$C_m \ge -0.092\tag{6}$$

and

$$A \ge A_{baseline}.$$
 (7)

x is the DV vector, while **l** and **u** are the lower and upper bounds, respectively, of each DV. A is the cross-sectional area of the airfoil non-dimensionalised with the square of the chord length (c). $A_{baseline}$ is the baseline area of the airfoil with a value of $0.07787c^2$.

B. Design variables

B-spline [49, 50] with eight control points was used to parameterize the RAE 2822 airfoil. The control points were only allowed to move in the vertical direction. Half of these control points were used to change the shape of the upper surface of the airfoil, while the other half the lower surface. The x/c-locations of these control points are $\mathbf{x}_c = [\mathbf{x}_{c,u}; \mathbf{x}_{c,l}]^T = [0.0 \ 0.15 \ 0.45 \ 0.80; \ 0.0 \ 0.35 \ 0.60 \ 0.90]^T$. The initial design variable vector is $\bar{\mathbf{x}}^{(0)} = [\bar{\mathbf{x}}_u^{(0)}; \bar{\mathbf{x}}_l^{(0)}]^T = [0.0175 \ 0.0498 \ 0.0688 \ 0.0406; \ -0.0291 \ -0.0679 \ -0.0384 \ 0.0054]^T$. The lower bound of \mathbf{x} is set to $\mathbf{l} = [0.0149 \ 0.0423 \ 0.0585 \ 0.0345; \ -0.0334 \ -0.0781 \ -0.0441 \ -0.0046]^T$, and the upper bound is set to $\mathbf{u} = [0.0201 \ 0.0572 \ 0.0572 \ 0.0791 \ 0.0467; \ -0.0247 \ -0.0577 \ -0.0326 \ 0.0062]^T$.

C. CFD setup and validation

To simulate the flow around the airfoil, an implicit density based solver in Stanford University Unstructured (SU2) [51] is used to solve the Reynolds averaged Navier Stokes (RANS) equations with the Spalart-Allmaras [52] turbulence model. Far field pressure and temperature are set to 39,313.85 Pa and 288.15 K, respectively. The Reynolds number (Re) used is $6.5 \cdot 10^6$. A no-slip wall boundary condition is set to the surface of the airfoil. The convective fluxes are calculated using the second order Jameson-Schmidt-Turkel (JST) scheme [53].

An o-grid mesh (Fig. 2) with the outer boundary set to 55c from the airfoil is generated using pyHyp [4, 5, 54]. The y+ was set to less than 1 in order to capture boundary layer physics as accurately as possible. Four different mesh sizes with increasing number of cells are generated (Table 1).

The CFD setup and the mesh is validated with case 9 from Cook et al. [55]. The convergence criteria is set to a minimum of either the total iterations specified in Table 1 or till the absolute difference in C_d between the last 150 iteration falls below 10^{-6} . For benchmark case II, the total number of iterations is changed to those specified in Table 2. For both these cases, the fixed C_l mode in SU2 is used. The Mach number and C_l is set to 0.73 and 0.803 as well as 0.734 and 0.824 for the validation case and benchmark case II, respectively. The remaining CFD setup and the meshes is the same as the validation case.

Table 1 shows the CFD results when compared to experimental data for the validation case. The meshes over-predict the C_d . Mesh 3 is around 2 drag counts higher than the experimental case, while mesh 4 is less than 1 drag count higher. Table 2 summarizes the mesh independence study for benchmark case II. Mesh 4 takes about 10 times as long to simulate than mesh 3. Based on the validation cases above, it is safe to assume that mesh 3 would work as an accurate HF model. For the LF model, mesh 1 was used. However, the 4^{th} order artificial dissipation coefficient in the JST scheme was changed from 0.02 to 0. The maximum number of iteration was reduced to 8,000. This setup helped improve convergence of the CFD simulations for the various shapes generated during the sampling of the design space. The simulation time decreased to 2.3 minutes and a drag value of 219.3 counts was obtained. Figure 3 (a) shows the Mach number contours simulated using mesh 3. The shock wave can be clearly seen where the contour changes color from red to green. Figure 3 (b) shows the pressure coefficient (C_p) over the airfoil. A steep rise in C_p is noticeable around the shock.

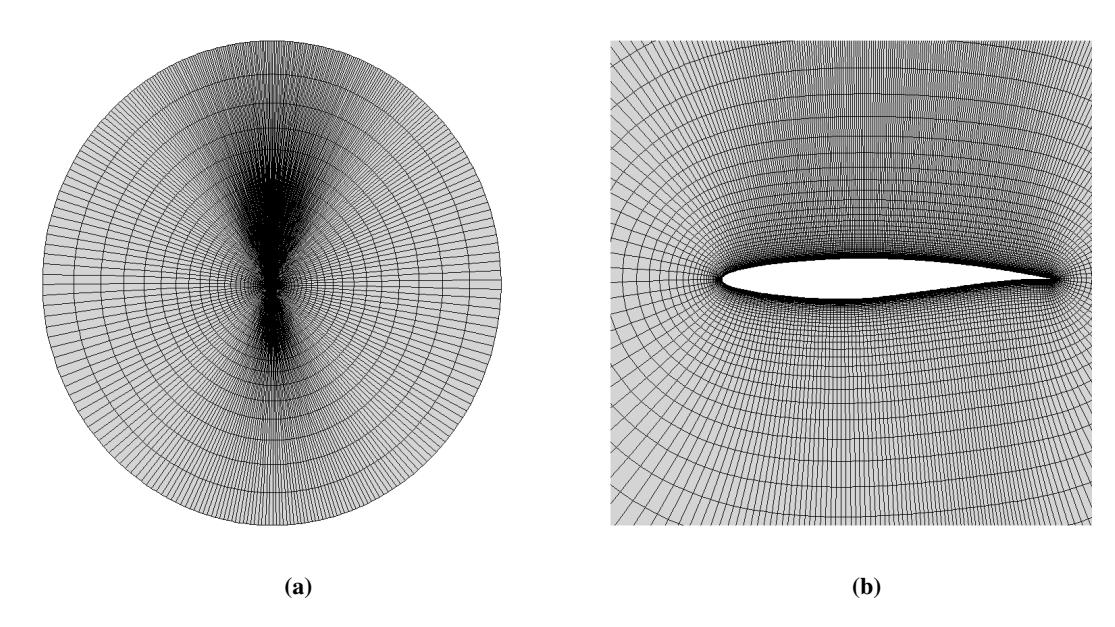


Figure 2 O-grid for benchmark case II: (a) domain, (b) near airfoil.

Table 1 Grid convergence study for the validation case

Mesh	Number of cells	C_d , counts	x/c	Max Iter	Simulation time, min
1	8,544	211.2	0.49	12,000	3.4*
2	33,696	177.1	0.52	12,000	9.4 **
3	133,536	170.1	0.52	20,000	47.4**
4	525,096	168.8	0.52	20,000	171.3**
Exp	-	168.0	0.52	-	

^{*}Computed on a high-performance cluster with 32 processors. Flow solution only.

Table 2 Grid convergence study of the baseline shape for benchmark case II

Mesh	α , degrees	C_l , counts	C_d , counts	C_m	Max Iter	Simulation time, min
1	3.33	82.4	260.3	-0.0856	12,000	3.4*
2	2.82	82.4	210.4	-0.0972	12,000	9.8**
3	2.77	82.4	202.1	-0.0985	20,000	47.4**
4	2.77	82.4	200.7	-0.0984	60,000	510.3**

^{*}Computed on a high-performance cluster with 32 processors. Flow solution only.

D. Metamodel generation and validation

To generate the metamodels, the design space was sampled using LHS. Five sets of samples with an increasing number of samples in each set were created. The number of samples in each set are 19, 34, 79, 155 and 305 respectively. The HF and LF model was evaluated at all these DVs in order to obtain the corresponding HF and LF response, namely C_d and C_m . An additional sample set contain 463 sample points were generated and only the LF model was evaluated at these DVs. The final LF sample set was created by combining all these sample points resulting in a total of 1,055 LF sample points. To make sure that no two sample points from different sets were overlapping, a cluster radius of 10^{-3} was set and the norm of the difference between the DVs were calculated. Any point that fell below this cluster radius value was removed.

Two separate metamodels, one for the objective function and the other for the constraint function, was constructed

^{**}Computed on a high-performance cluster with 64 processors. Flow solution only.

^{**}Computed on a high-performance cluster with 64 processors. Flow solution only.

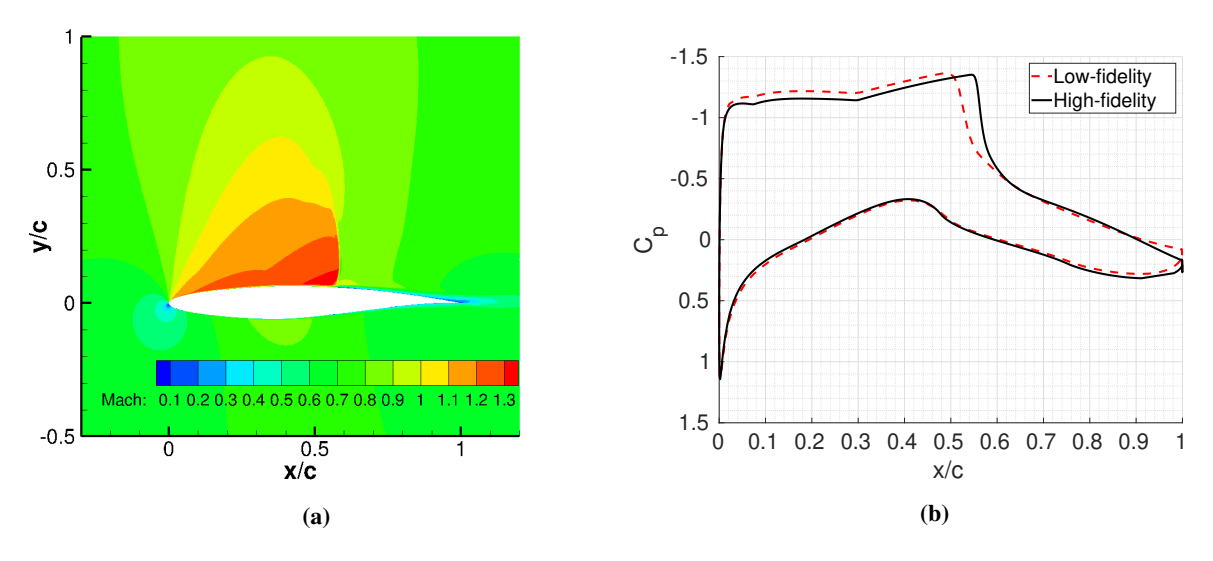


Figure 3 CFD results for RAE2822 airfoil: (a) Mach number contours (Mesh 3), (b) C_p profile (LF: mesh 1, HF: mesh 3).

and validated with 145 HF testing points. The global accuracy was measured using RMSE and NRMSE. Figures 4 and 5 show the RMSE and NRMSE on the drag and pitching moment coefficient metamodels, respectively. From Fig. 4, it can be seen that the multifidelity metamodels are significantly more accurate than the single fidelity metamodels for a small number of HF data. This difference in accuracy diminishes in the presence of higher number of HF data and even results in poorer global accuracy. In Fig. 5, the difference in accuracy between single and multifidelity metamodels is not as large as those noticed in the C_d metamodel for a low number of HF data points. This difference also decreases with incresing number of HF data points. However, even at high number of HF data points the multifidelity metamodels are more accurate. The global accuracy of $10\%\sigma_{\text{testing}}$ is reached with a fewer number of HF points on the pitching moment coefficient function than the drag coefficient function for all the metamodels. Also, the trends and values of the PC-Corkriging and Cokriging metamodels are similar.

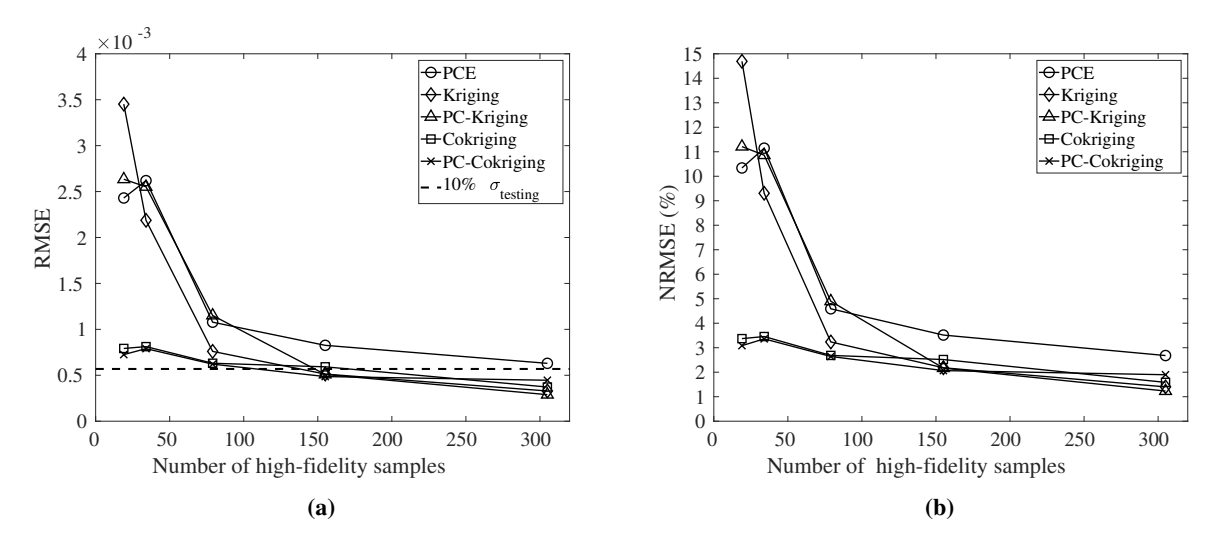


Figure 4 Drag coefficient metamodel validation: (a) RMSE, (b) NRMSE.

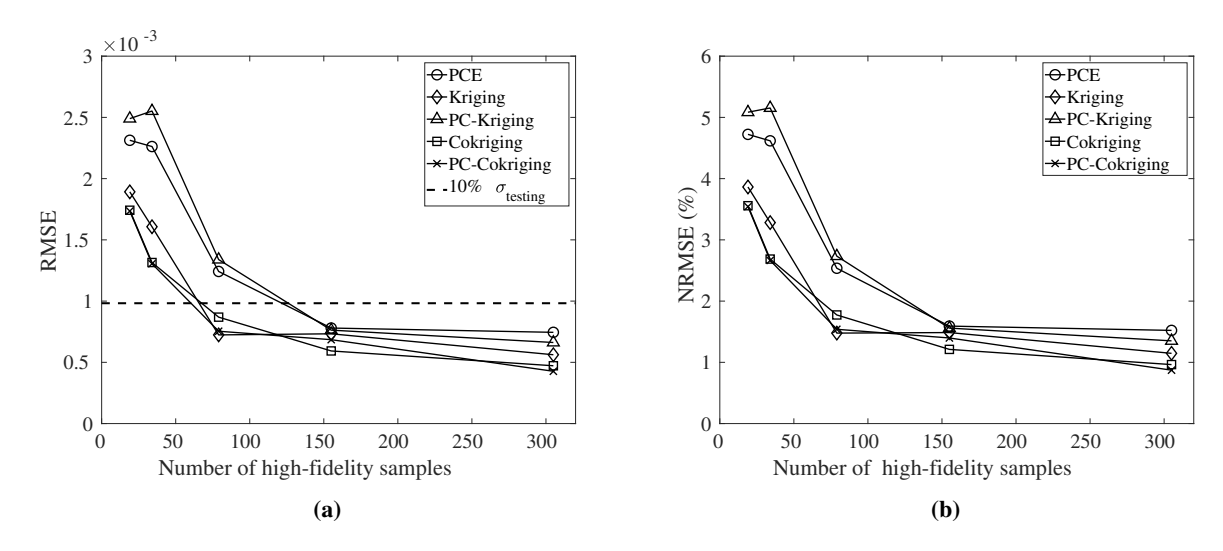


Figure 5 Pitching moment coefficient metamodel validation: (a) RMSE, (b) NRMSE.

E. Optimization results

The SLSQP gradient based optimizer with 40 initial starting points is used to find the minimum design. Previous study done by He et al. [4] show that benchmark case II is unimodal and has a global minimum. The metamodel constructed could have local minimums and this could prevent the optimizer from finding the true global minimum, hence 40 different starting points were used. The lowest objective function value found by SLSQP was then evaluated using CFD and the results are plotted in Fig. 6. Note that zero number of HF samples corresponds to the baseline design for all the plots in Fig. 6. The resulting optimized shapes are plotted in Fig. 7.

Figure 6 (a) shows the convergence of the argument \mathbf{x}^* varying with the number of HF samples. \mathbf{x}^* refers to the optimal value of the DVs for each data set. The suffix 'n' refers to the HF sample set. n equals to one corresponds to the HF sample set with 19 samples. Increasing n to two corresponds to 34 HF samples sets and so on. n equals to zero corresponds to the baseline case. These results are not uniformly decreasing even though the trend of the global accuracy is (cf. Figs. 4 and 5). This is because at the optima found, the local accuracy may vary between the metamodels. This inaccuracy affects the location of the optima predicted by the metamodels.

Figure 6 (b) shows the convergence of the objective function. Both Cokriging and PC-Cokriging multifidelity metamodels converge quickly to the optimum drag values. The single fidelity metamodels require at least 155 HF samples to converge. The optimum drag value predicted by the metamodels is around 129 drag counts and the differences between these values can be attributed to the local accuracy of the metamodels at the global mimimum. A difference of approximately 2 drag counts is noted between the metamodels. The trends and values of the objective function of the Cokriging and PC-Cokriging metamodels are similar.

The convergence of the constraint function is shown in Fig. 6 (c). Again, the multifidelity metamodels converge to the constraint value of -0.092 faster than the single fidelity models. For all but one case (PC-Kriging with 79 HF samples) this constraint is not violated. Note that the constraint function is not violated at the optima found from the metamodel. It is violate when the CFD simulation is run on the optima found. This again is attributed to local inaccuracy of the metamodel at the optima. Again, the Cokriging and PC-Cokriging metamodels have similar trends and values.

Figures 7 shows the baseline as well as all the optimized shapes obtained from the metamodels. What is immediately noticeable is that increasing the number of HF samples results in optimized shapes being more similar between the metamodels. Increasing the number of HF samples increases both the global and local accuracy at the optima. Between the leading edge and the mid chord on the suction side of the airfoil, the optimized airfoil has a lower curvature. This reduced the acceleration of air around on the suction side resulting a significantly lower shock strength (cf. Figs. 8 and 9).

Table 3 shows the results from the grid convergence study perform on the optimized shape predicted from the PC-Cokriging model generated from 155 HF sample points. Note that the mesh and CFD setup is the same as those performed on the baseline case (Table 2). There is a 1.4 drag count difference between mesh 3 and 4 on the baseline case. For the optimized shapes, this difference increased to 1.9 drag counts. This confirms that mesh 3 serves as an appropriate HF mesh.

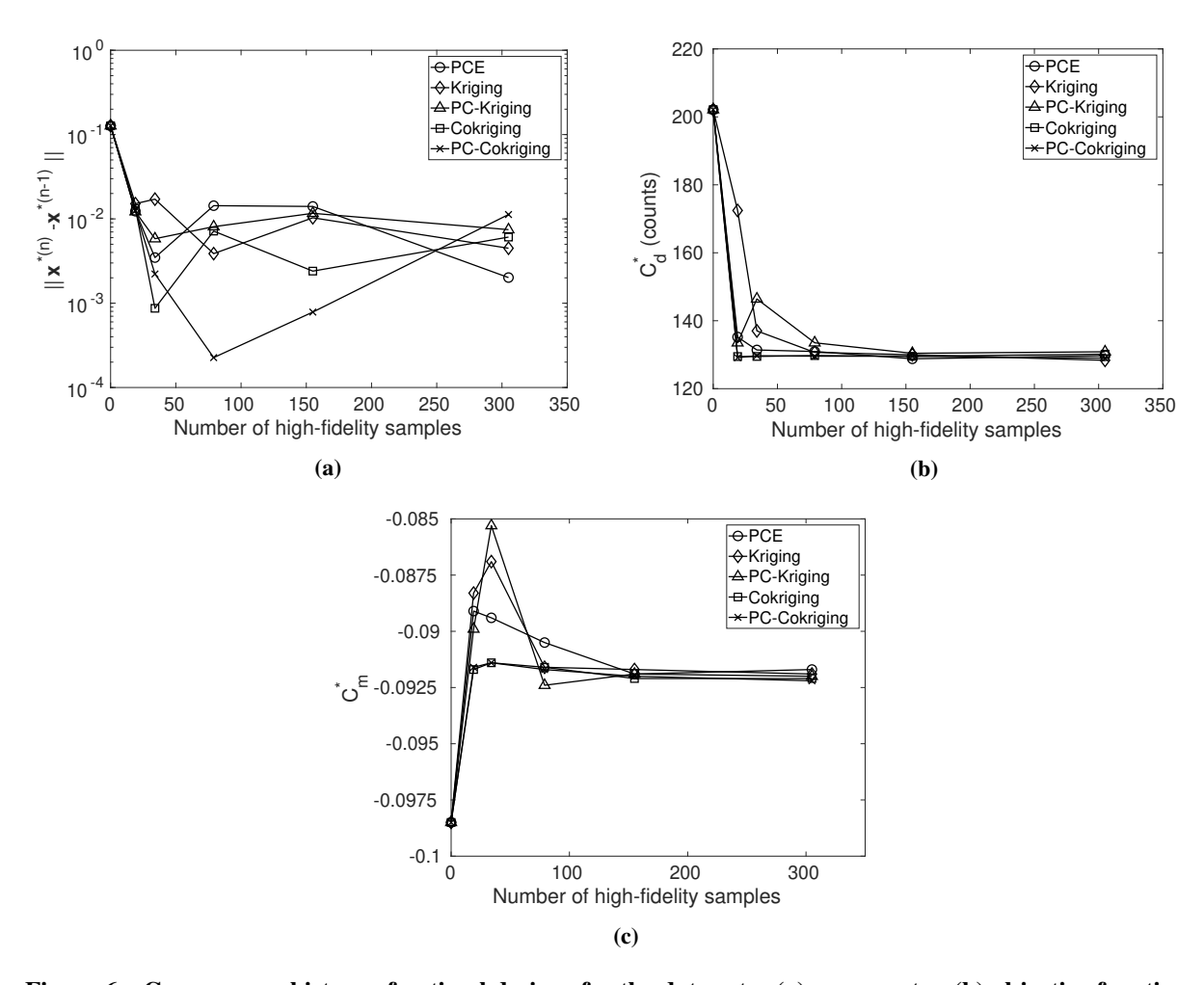


Figure 6 Convergence history of optimal designs for the data sets: (a) argument x, (b) objective function, (c) constraint function.

Table 3 Grid convergence study of the optimized shape for benchmark case II

Mesh	α , degrees	C_l , counts	C_d , counts	C_m
1	3.30	82.4	183.7	-0.0779
2	2.82	82.4	138.7	-0.0905
3	2.76	82.4	129.6	-0.0920
4	2.76	82.4	127.6	-0.0920

Figure 8 shows the Mach number contour on the baseline and optimized shapes. The decrease in strength of the shock wave can be seen. Figure 9 shows the difference in pressure coefficient and skin friction coefficient profile between the baseline shape and the optimized shaped. The strength of the shock has significantly reduced. However, the shock has not completely been eliminated. In Fig. 9 (a), the rise in pressure coefficient around mid chord is lower for the optimized shape than the baseline shape. This corresponds to a smaller drop in skin friction coefficient at the same location for the optimized shape compared to the baseline shape. The drop is velocity past the shock wave is lower for the optimized shape due to the weaker shock wave, corresponding to higher skin friction coefficient downstream of the shock

Table 4 show results obtained for benchmark case II from literature. In most of the cases, the shock wave has been completely eliminated, which is not the case for this study. However, comparing to other cases where B-spline control

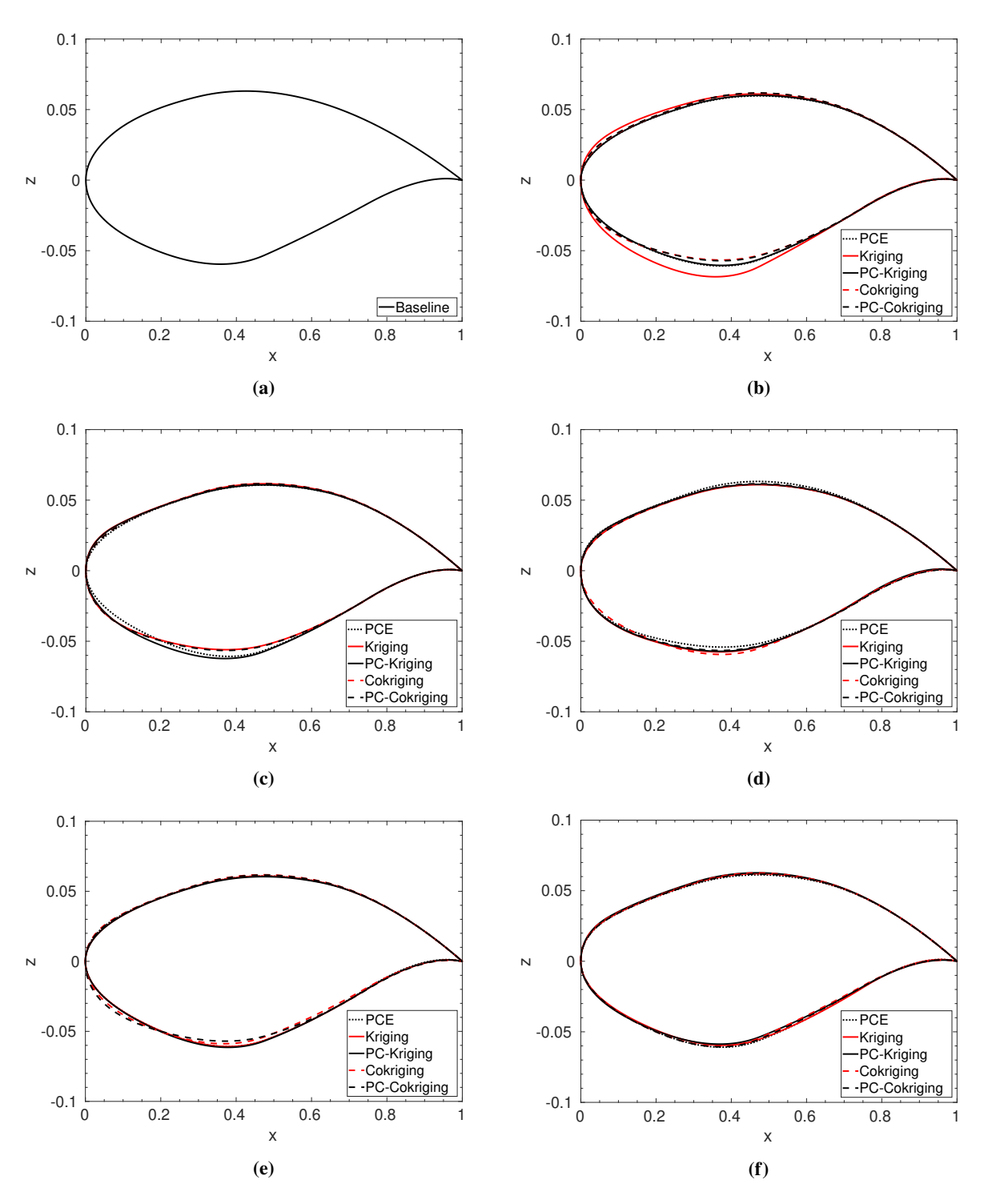


Figure 7 Airfoil shapes: (a) baseline, optimized: (b) 19 samples, (c) 34 samples, (d) 79 samples, (e) 155 samples, (f) 305 samples.

points were used to parameterize the airfoil, it can be seen that the number of DVs used are nearly double. This implies that eight B-spline control points cannot be used to capture a shock free optimum shape for benchmark case II.

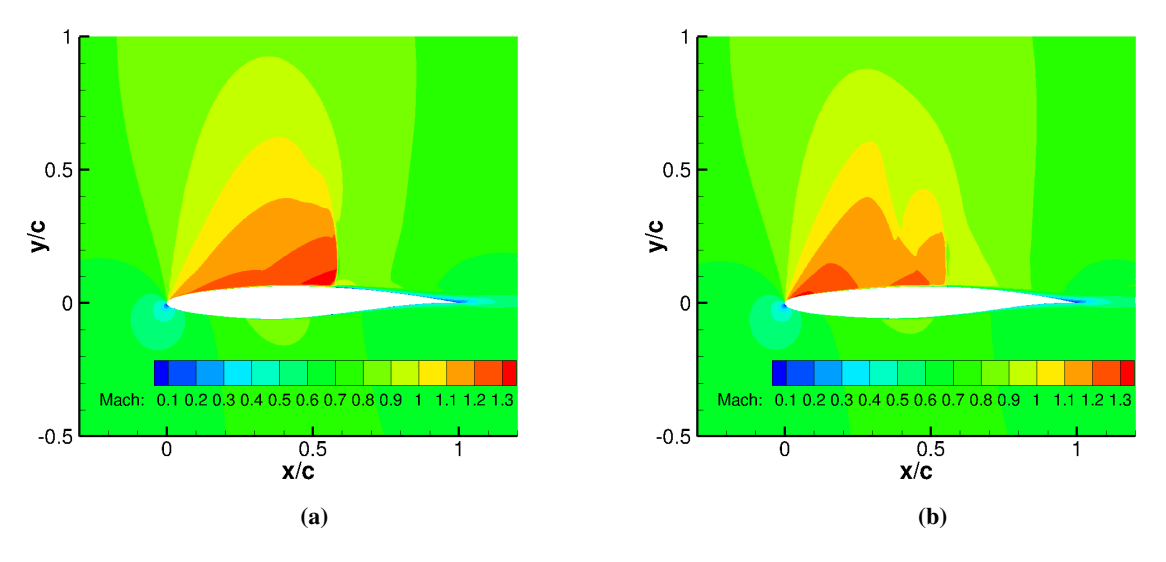


Figure 8 Mach number contours: (a) baseline, (b) optimized.

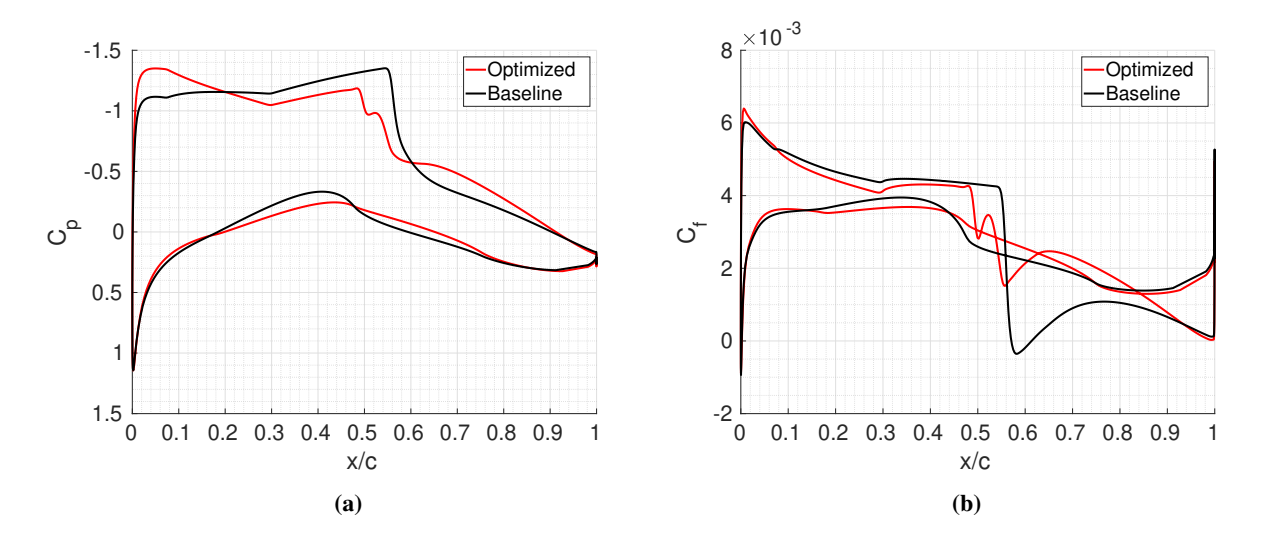


Figure 9 Baseline vs optimized results: (a) pressure coefficient profile, (b) skin friction coefficient profile.

Table 4 Benchmark case II optimization results compared to those in literature.

G. 1	D	N_{DV}	D 1:	0 1	CI	C1 1 C
Study	Parameterization method		Baseline	Optimized	Change	Shock free
Lee et al. [36]	B-spline		234.4	131.8	-102.6	Yes
Current work	B-spline	8	200.7	127.6	-73.1	No
Anderson et al. [33]	Direct manipulation approach		196.0	124.0	-72.0	No
He et al. [4]	Free form deformation	40	194.4	108.9	-85.5	Yes
Zhang et al. [35]	Class-shape function transformation (CST)		194.1	103.6	-90.5	Yes
Bisson and Nadarajah [34]	B-spline	16	177.8	102.3	-75.5	Yes

IV. Conclusion

In this study, the PC-Cokriging model, which a multivariate version of the PC-Kriging model, is applied to the ADODG benchmark case II to find the minimum drag subject to area and pitching moment constraint. The PC-Kriging model combines the PCE and the Kriging models. The regression-based PCE captures the global trend function, while the

interpolation-based Kriging model captures the local deviations. The PC-Cokriging model's construction is similar to that of the Cokriging model.

The metamodels are first constructed with five different sets of samples, each with an increasing number of HF samples. The global accuracy of these metamodels are compared in terms of the RMSE and NRMSE for both the objective and constraint function. For a low number of HF samples, the multifidelity models are more accurate than the single fidelity metamodels. This difference in accuracy decreases with increasing number of HF data. This highlights the benefit of using multifidelity metamodels in the absence of large amounts of HF data. Differences in global accuracy between Cokriging and PC-Cokriging is insignificant in this deterministic case.

Once the global accuracy was measured, the gradient based SLSQP was used to find the minima from the metamodels. At this optima the CFD simulations were rerun to find the objective and constraint values. The multifidelity metamodels converge faster for both the objective and constraint function when compared to the single fidelity metamodels. A significant reduction in shock strength is achieved through the optimization process. However, the optima is not shock free. The use of eight B-spline control points were noted as the reason for this. In the future, this study would need to be redone with a higher number of DVs.

This study highlights the benefit of using multidelity metamodels in the absence of high number of HF data. While global accuracy improves with increasing number of HF samples, the local accuracy at optima may or may not. The use of expected improvement might prove to be a better approach to finding the optima while improving both global and local accuracy. This might even need a low number HF samples to find the minimum. This however needs to be studied.

The current study has been perform for a deterministic case. In the future, this would need to be expanded to study "robust design" to include parametric uncertainties. This study could entail reducing the drag for varying flow and geometry parameters such as Mach number, lift coefficient and thickness distribution. Here, it is expected that PC-Cokriging will outperform Cokriging.

Acknowledgements

The first two authors are supported by NSF award number 1846862.

References

- [1] Skinner, S., and Zare-Behtash, H., 'State-of-the-art in aerodynamic shape optimisation methods,' *Applied Soft Computing*, Vol. 62, 2018, pp. 933 962. doi:https://doi.org/10.1016/j.asoc.2017.09.030.
- [2] Mader, C. A., and Martins, J. R. R. A., 'Derivatives for Time-Spectral Computational Fluid Dynamics Using an Automatic Differentiation Adjoint,' *AIAA Journal*, Vol. 50, 2012, pp. 2809–2819. doi:10.2514/1.J051658.
- [3] Leung, T. M., and Zingg, D. W., 'Aerodynamic shape optimization of wings using a parallel newton-krylov approach,' *AIAA Journal*, Vol. 50, No. 3, 2012, pp. 540–550.
- [4] He, X., Li, J., Mader, C. A., Yildirim, A., and Martins, J. R. R. A., 'Robust aerodynamic shape optimization—from a circle to an airfoil,' *Aerospace Science and Technology*, Vol. 87, 2019, p. 48–61. doi:10.1016/j.ast.2019.01.051.
- [5] Secco, N. R., and Martins, J. R. R. A., 'RANS-based aerodynamic shape optimization of a strut-braced wing with overset meshes,' *Journal of Aircraft*, Vol. 56, 2019, pp. 217–227. doi:10.2514/1.C034934.
- [6] Yu, Y., Lyu, Z., Xu, Z., and Martins, J. R., 'On the influence of optimization algorithm and initial design on wing aerodynamic shape optimization,' *Aerospace Science and Technology*, Vol. 75, 2018, pp. 183 199.
- [7] Lyu, Z., Kenway, G. K. W., and Martins, J. R. R. A., 'Aerodynamic shape optimization investigations of the Common Research Model Wing benchmark,' *AIAA Journal*, Vol. 53, No. 4, 2015, pp. 968–985. doi:10.2514/1.J053318.
- [8] Chen, S., Lyu, Z., Kenway, G. K. W., and Martins, J. R. R. A., 'Aerodynamic Shape Optimization of Common Research Model Wing–Body–Tail Configuration,' *Journal of Aircraft*, Vol. 53, No. 1, 2016, pp. 276–293. doi:10.2514/1.C033328.
- [9] Jonsson, I. M., Leifsson, L., Koziel, S., Tesfahunegn, Y. A., and Bekasiewicz, A., 'Trawl-door Shape Optimization by Space-mapping-corrected CFD Models and Kriging Surrogates,' *Procedia Computer Science*, Vol. 80, 2016, pp. 1061 – 1070, International Conference on Computational Science 2016, ICCS 2016, 6–8 June 2016, San Diego, California, USA. doi:https://doi.org/10.1016/j.procs.2016.05.409.
- [10] Koziel, S., Tesfahunegn, Y. A., and Leifsson, L., 'Variable-fidelity CFD models and co-Kriging for expedited multi-objective aerodynamic design optimization,' Vol. 33, 2016, pp. 2320-2338. doi:10.1108/EC-09-2015-0277.

- [11] Amrit, A., Leifsson, L., Koziel, S., and Tesfahunegn, Y. A., 'Efficient Multi-Objective Aerodynamic Optimization by Design Space Dimension Reduction and Co-Kriging,' 17th AIAA/ISSMO Multidisciplinary Analysis and Optimization Conference, 13-17 June 2016, Washington, D.C., USA. doi:10.2514/6.2016-3515.
- [12] Shah, H., Hosder, S., Koziel, S., Tesfahunegn, Y. A., and Leifsson, L., 'Multi-fidelity robust aerodynamic design optimization under mixed uncertainty,' *Aerospace Science and Technology*, Vol. 45, 2015, pp. 17 - 29. doi:https://doi.org/10.1016/j.ast.2015. 04.011.
- [13] Tesfahunegn, Y. A., Koziel, S., Gramanzini, J.-R., Hosder, S., Han, Z.-H., and Leifsson, L., 'Application of Direct and Surrogate-Based Optimization to Two-Dimensional Benchmark Aerodynamic Problems: A Comparative Study,' AIAA Paper 2015-0265, 53rd AIAA Aerospace Sciences Meeting, 2015, pp. 5–9.
- [14] Tao, J., and Sun, G., 'Application of deep learning based multi-fidelity surrogate model to robust aerodynamic design optimization,' *Aerospace Science and Technology*, Vol. 92, 2019, pp. 722 737. doi:https://doi.org/10.1016/j.ast.2019.07.002.
- [15] Yan, X., Zhu, J., Kuang, M., and Wang, X., 'Aerodynamic shape optimization using a novel optimizer based on machine learning techniques,' *Aerospace Science and Technology*, Vol. 86, 2019, pp. 826 835. doi:https://doi.org/10.1016/j.ast.2019.02.003.
- [16] Bouhlel, M. A., Bartoli, N., Regis, R. G., Otsmane, A., and Morlier, J., 'Efficient global optimization for high-dimensional constrained problems by using the Kriging models combined with the partial least squares method,' *Engineering Optimization*, Vol. 0, No. 0, 2018, pp. 1–16. doi:10.1080/0305215X.2017.1419344.
- [17] Queipo, N. V., Haftka, R. T., Shyy, W., Goel, T., Vaidyanathan, R., and Tucker, P. K., 'Surrogate-Based Analysis and Optimization,' *Progress in Aerospace Sciences*, Vol. 41, No. 1, 2005, pp. 1–28. doi:10.1016/j.paerosci.2005.02.001.
- [18] Queipo, N., Pintos, S., and Nava, E., 'Setting Targets in Surrogate-Based Optimization,' *Journal of Global Optimization*, Vol. 55, No. 4, 2013, pp. 857–875. doi:10.1007/s10898-011-9837-4.
- [19] Peherstorfer, B., Willcox, K., and Gunzburger, M., 'Survey of Multifidelity Methods in Uncertainty Propagation, Inference, and Optimization,' Society for Industrial and Applied Mathematics, Vol. 60, No. 3, 2018, pp. 550–591. doi:https://doi.org/10.1137/ 16M1082469.
- [20] Forrester, A. I. J., and Keane, A. J., 'Recent Advances in Surrogate-Based Optimization,' *Progress in Aerospace Sciences*, Vol. 45, No. 1-3, 2009, pp. 50–79. doi:10.1016/j.paerosci.2008.11.001.
- [21] Krige, D. G., 'A Statistical Approach to Some Basic Mine Valuation Problems on the Witwatersrand,' *Journal of the Chemical, Metallurgical and Mining Engineering Society of South Africa*, Vol. 52, No. 6, 1951, pp. 119–139.
- [22] Matheron, G., 'Principles of geostatistics,' Economic Geology, Vol. 58, 1963, pp. 1246–1266. doi:10.2113/gsecongeo.58.8.1246.
- [23] Sacks, J., Welch, W., Michell, J. T., and Wynn, P. H., 'Design and Analysis of Computer Experiments,' *Statistical Science*, Vol. 4, 1989, pp. 409–423. doi:10.1214/ss/1177012413.
- [24] Blatman, G., 'Adaptive Sparse Polynomial Chaos Expansion for Uncertainty Propagation and Sensitivity Analysis,' *Ph.D. Thesis, Blaise Pascal University Clermont II. 3, 8, 9,* 2009.
- [25] Smola, A. J., and Scholkopf, B., 'A Tutorial on Support Vector Regression,' Statistics and Computing, Vol. 14, 2004, pp. 199–222. doi:10.1023/B:STCO.0000035301.49549.88.
- [26] Alexandrov, N. M., Lewis, R. M., Gumbert, C. R., Green, L. L., and Newman, P. A., 'Approximation and Model Management in Aerodynamic Optimization with Variable-Fidelity Models,' *Journal of Aircraft*, Vol. 38, No. 6, 2001, pp. 1093–1101. doi:10.2514/2.2877.
- [27] Rathinam, M., and Petzold, L., 'A New Look at Proper Orthogonal Decomposition,' *SIAM Journal on Numerical Analysis*, Vol. 41, No. 5, 2003, pp. 1893–1925. doi:10.1137/S0036142901389049.
- [28] Du X. and Leifsson L., 'Multifidelity Modeling by Polynomial Chaos-Based Cokriging to Enable Efficient Model-Based Reliability Analysis of NDT Systems,' *submitted to Springer Journal of Nondestructive Evaluation*, 2019.
- [29] Du, X., and Leifsson, L., 'Efficient Uuncertainty Propagation for MAPOD via Polynomial Chaos-based Kriging,' *Engineering Computations*, Vol. ahead-of-print, 2019. doi:10.1108/EC-04-2019-0157.
- [30] Schobi, R., Sudret, B., and Wiart, J., 'Polynomial-chaos-based Kriging,' *International Journal of Uncertainty Quantification*, Vol. 5, 2015, pp. 193–206.

- [31] Schobi, R., Sudret, B., and Marelli, S., 'Rare event estimation using Polynomial-Chaos-Kriging,' ASCE-ASME Journal of Risk and Uncertainty in Engineering Systems, Part A: Civil Engineering, 2016.
- [32] Carrier, G., Destarac, D., Dumont, A., Meheut, M., Din, I. S. E., Peter, J., Khelil, S. B., Brezillon, J., and Pestana, M., 'Gradient-Based Aerodynamic Optimization with the elsA Software,' in 52nd Aerospace Sciences Meeting, 2014. doi:10.2514/6.2014-0568.
- [33] Anderson, G. R., Nemec, M., and Aftosmis, M. J., 'Aerodynamic Shape Optimization Benchmarks with Error Control and Automatic Parameterization,' in 53rd AIAA Aerospace Sciences Meeting, 2015. doi:10.2514/6.2015-1719.
- [34] Bisson, F., and Nadarajah, S., 'Adjoint-Based Aerodynamic Optimization Framework,' in 52nd Aerospace Sciences Meeting, 2014. doi:10.2514/6.2014-0412.
- [35] Zhang, Y., Han, Z.-H., Shi, L., and Song, W.-P., 'Multi-round Surrogate-based Optimization for Benchmark Aerodynamic Design Problems,' in 54th AIAA Aerospace Sciences Meeting, 2016. doi:10.2514/6.2016-1545.
- [36] Lee, C., Koo, D., Telidetzki, K., Buckley, H., Gagnon, H., and Zingg, D. W., 'Aerodynamic Shape Optimization of Benchmark Problems Using Jetstream,' in 53rd AIAA Aerospace Sciences Meeting, 2015. doi:10.2514/6.2015-0262.
- [37] Poole, D. J., Allen, C. B., and Rendall, T., 'Control Point-Based Aerodynamic Shape Optimization Applied to AIAA ADODG Test Cases,' in 53rd AIAA Aerospace Sciences Meeting, 2015. doi:10.2514/6.2015-1947.
- [38] Gariepy, M., Trepanier, J.-Y., Petro, E., Malouin, B., Audet, C., LeDigabel, S., and Tribes, C., 'Direct Search Airfoil Optimization Using Far-Field Drag Decomposition Results,' in 53rd AIAA Aerospace Sciences Meeting, 2015. doi:10.2514/6.2015-1720.
- [39] Wiener, N., 'The Homogeneous Chaos,' American Journal of Mathematics, Vol. 60, No. 4, 1938, pp. 897–936. doi: 10.2307/2371268.
- [40] Shields, M. D., and Zhang, J., 'The generalization of Latin Hypercube Sampling,' Reliability Engineering & System Safety, Vol. 148, 2016, pp. 96–108. doi:https://doi.org/10.1016/j.ress.2015.12.002.
- [41] Forrester, I. J. A., Sobester, A., and Keane, J. A., 'Multi-Fidelity Optimization via Surrogate Modelling,' Proceedings of the Royal Society A Mathematical Physical and Engineering Sciences, Vol. 463, No. 2088, 2007, pp. 3251–3269. doi:10.1098/rspa.2007.1900.
- [42] Kennedy, C. M., and O'Hagan, A., 'Predicting the Output from a Complex Computer Code When Fast Approximations are available,' *Biometrika*, Vol. 87, No. 1, 2000, pp. 1–13. doi:10.1093/biomet/87.1.1.
- [43] Du, X., and Leifsson, L., 'Multifidelity Model-Assisted Probability of Detection via Cokriging,' *NDT & E International*, Vol. 108, 2019, p. 102156. doi:https://doi.org/10.1016/j.ndteint.2019.102156.
- [44] Forrester, J. I. A., Sobester, A., and Keane, J. A., 'Engineering Design via Surrogate Modelling: A Practical Guide,' *Engineering Design via Surrogate Modelling: A Practical Guide*, 2008, pp. 33–76. doi:10.1002/9780470770801.
- [45] Efron, B., Hatie, T., Johnstone, I., and Tibshirani, R., 'Least Angle Regression,' *The Annals of Statistics*, Vol. 32, No. 2, 2004, pp. 407–499. doi:10.1214/00905360400000067.
- [46] Ryu, J., Kim, K., Lee, T., and Choi, D., 'Kriging Interpolation Methods in Geostatistics and DACE Model,' *Korean Society of Mechanical Engineering International Journal*, Vol. 16, No. 5, 2002, pp. 619–632. doi:10.1007/BF03184811.
- [47] Gneiting, T., Kleiber, W., and Schlather, M., 'Matern Cross-Covariance Functions for Multivariate Random Fields,' *Journal of the American Statistical Association*, Vol. 105, No. 491, 2010, pp. 1167–1177. doi:http://dx.doi.org/10.1198/jasa.2010.tm09420.
- [48] Virtanen, P., Gommers, R., Oliphant, T. E., Haberland, M., Reddy, T., Cournapeau, D., Burovski, E., Peterson, P., Weckesser, W., Bright, J., van der Walt, S. J., Brett, M., Wilson, J., Jarrod Millman, K., Mayorov, N., Nelson, A. R. J., Jones, E., Kern, R., Larson, E., Carey, C., Polat, İ., Feng, Y., Moore, E. W., Vand erPlas, J., Laxalde, D., Perktold, J., Cimrman, R., Henriksen, I., Quintero, E. A., Harris, C. R., Archibald, A. M., Ribeiro, A. H., Pedregosa, F., van Mulbregt, P., and Contributors, 'SciPy 1.0–Fundamental Algorithms for Scientific Computing in Python,' arXiv e-prints, 2019, arXiv:1907.10121.
- [49] Leifsson, L., Koziel, S., and Kurgan, P., 'Automated Low-Fidelity Model Setup for Surrogate-Based Aerodynamic Optimization,' *Solving Computationally Expensive Engineering Problems*, Vol. 97, 2014, pp. 87–111.
- [50] Samareh, J. A., 'Survey of Shape Parameterization Techniques for High-Fidelity Multidisciplinary Shape Optimization,' AIAA Journal, Vol. 39, No. 5, 2001, pp. 877—884.

- [51] Economon, T. D., Palacios, F., Copeland, S. R., Lukaczyk, T. W., and Alonso, J. J., 'SU2: An Open-Source Suite for Multiphysics Simulation and Design,' *AIAA Journal*, Vol. 54, No. 3, 2015, pp. 828–846.
- [52] Spalart, P., and Allmaras, S., 'A One-Equation Turbulence Model for Aerodynamic Flows,' 30th Aerospace Sciences Meeting and Exhibit, 06 January 1992 - 09 January 1992, Reno, NV, U.S.A. doi:10.2514/6.1992-439.
- [53] Jameson, A., Schmidt, W., and Turkel, E., 'Numerical Solution of the Euler Equations by Finite Volume Methods Using Runge-Kutta Time-Stepping Schemes,' *AIAA 14th Fluid and Plasma Dynamic Conference*, Vol. 1981–1259, Palo Alto, CA, June 23-25, 1981. doi:10.2514/6.1981-1259.
- [54] Chan, W. M., and Steger, J. L., 'Enhancements of a three-dimensional hyperbolic grid generation scheme,' Applied Mathematics and Computation, Vol. 51, No. 2, 1992, pp. 181 – 205. doi:https://doi.org/10.1016/0096-3003(92)90073-A.
- [55] Cook, P. H., McDonald, M. A., and Firmin, M. C. P., 'Aerofoil RAE 2822 Pressure Distributions, and Boundary Layer and Wake Measurements,' *Experimental Data Base for Computer Program Assessment, AGARD Report AR 138*, 1979.